Charge and anion ordering in the quasi-one-dimensional organic conductor $(TMTTF)_2NO_3$

Olga Iakutkina, Lena Nadine Majer, Guilherme Gorgen Lesseux, Gabriele Untereiner, and Martin Dressel
1. Physikalisches Institut, Universität Stuttgart, 70569 Stuttgart, Germany

(Received 17 January 2021; revised 15 March 2021; accepted 8 April 2021; published 14 April 2021)

The quasi-one-dimensional organic conductors $(TMTTF)_2X$ with noncentrosymmetric anions commonly undergo charge- and anion-order transitions upon cooling. While for compounds with tetrahedral anions ($X = BF_4^-$, ReO_4^-, and ClO_4^-) the charge-ordered phase is rather well understood, the situation is less clear in the case of planar triangular anions, such as $(TMTTF)_2NO_3$. Here we explore the electronic and structural transitions by transport experiments, optical, and magnetic spectroscopy. This way we analyze the temperature dependence of the charge imbalance 2δ and an activated behavior of $\rho(T)$ with $\Delta_{CO} \approx 530$ K below $T_{CO} = 250$ K. Since $(TMTTF)_2NO_3$ follows the universal relation between charge imbalance 2δ and size of the gap Δ_{CO}, our findings suggest that charge order is determined by TMTTF stacks with little influence of the anions. Clear signatures of anion ordering are detected at $T_{AO} = 50$ K. The tetramerization affects the dc transport, the vibrational features of donors and acceptors, and leads to formation of spin singlets.

DOI: 10.1103/PhysRevB.103.155126

I. INTRODUCTION

In low-dimensional electron systems, the influence of electronic correlations becomes more pronounced and may govern the effects of the crystal lattice [1,2]. A prime example is given by the quasi-one-dimensional Fabre salts $(TMTTF)_2X$, where TMTTF stands for tetramethyltetratiofulvalene and X is a monovalent anion. By stoichiometry these systems possess three-quarter-filled conduction bands, but dimerization leads to effectively half-filling. Although they are supposed to be metals according to their band structure, electron-electron interaction leads to charge localization. Furthermore, different broken-symmetry ground states can be realized depending on the subtle interplay of charge, spin, and lattice degrees of freedom [3–7].

In $(TMTTF)_2X$ salts with octahedral anions ($X = PF_6^-$, AsF_6^-, SbF_6^-, NbF_6, and TaF_6^-), charge order (CO) was extensively investigated by several methods [8–13]. A regular 1010 charge pattern develops along the molecular stacking axis a below the transition temperature T_{CO}. For noncentrosymmetric anions ($X = BF_4^-$, ReO_4^-, and ClO_4^-), the situation is more complicated because—in addition to the CO phase transition—the anions may order (AO) in an alternating fashion at low temperatures, which leads to a tetramerization of the donor molecules [6,14–18] and a doubling of the charge pattern to alternating sequence 0110 below T_{AO}. Despite the different anion size, for all these compounds a universal relation between charge imbalance 2δ, ordering temperature T_{CO}, and charge gap Δ_{CO} was revealed [19], which implies that the CO state is intrinsic for the TMTTF stacks and is mainly determined by a competition between the intersite Coulomb repulsion V and the bandwidth W.

So far, the detailed investigation was confined to $(TMTTF)_2X$ salts with tetrahedral anions, while other symmetries were considered only incidentally. For $(TMTTF)_2SCN$ with linear anions, CO coincides with the ordering of the noncentrosymmetric anions [13]. The situation is even more complex in the case of $X = NO_3^-$, where the planar anions have trigonal symmetry. For decades it was discussed in the community whether or not CO occurs in $(TMTTF)_2NO_3$ [15,20]. Like other salts with noncentrosymmetric anions, the salt undergoes an AO transition around 50 K, which was identified by x-ray diffraction and electron spin resonance (ESR) measurements [17,20]. Recent ESR data provided further evidence for the stabilization of a CO state below 250 K [21]. Here we present the results of detailed spectroscopic investigations of the charge distribution in $(TMTTF)_2NO_3$ in the CO and AO states.

II. MATERIALS AND EXPERIMENTS

The aciculate single crystals of $(TMTTF)_2NO_3$ used for our investigations were grown by standard electrochemical methods [22]. The organic TMTTF donor molecules are stacked along the crystallographic a axis; these stacks are separated by monovalent NO_3^- anions in the c direction, as displayed in Fig. 1(a). In the normal state at ambient condition, the molecules are slightly dimerized along the chains with intra- and interdimer distances d_1 and d_2, respectively.

At elevated temperature, the planar NO_3^- anions exhibit orientational disorder with four possible arrangements for the nitrate ions, with each possible orientation rotated on 30° with respect to each other, as indicated in Fig. 1(c). Since there are in total 12 possible positions for oxygen, the anion almost resembles a nitrogen atom surrounded by an oxygen ring [23]. At reduced temperatures, below T_{AO}, the anions arrange in an orderly fashion. For the metallic analog $(TMTSF)_2NO_3$, which does not exhibit any ordering down to $T_{AO} = 45$ K, the crystal structure in the AO state was resolved;

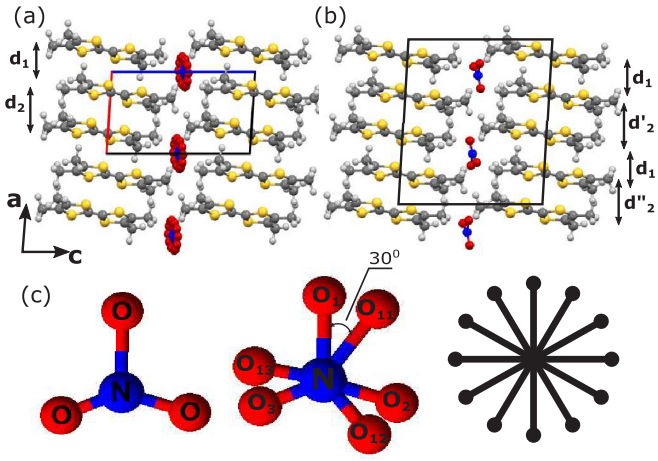

FIG. 1. (a) Crystal structure of $(TMTTF)_2NO_3$ where TMTTF stands for tetramethyltetrathiafulvalene at the normal state with finite dimerization and disordered anions, d_1 and d_2 are intra- and inter-dimmers distances respectively. (b) Suggested low-temperature state with alternating orientation of the anions that leads to a doubling of the unit cell and tetramerization along the TMTTF molecular stack. (c) From the left to the right shape of the planar NO_3^- anion, the difference between two anion orientations, and all possible orientations are shown.

here, the AO leads to a doubling of the unit cell [24,25]. For $(TMTTF)_2NO_3$ we expect that the AO leads to tetramerization of the TMTTF molecules with distances d_1, d_2', d_1, and d_2'' as illustrated in Fig. 1(b).

In order to characterize the compound by dc resistivity measurements, two contacts were attached along the a direction by carbon paste. To ensure good thermal contact, the samples were anchored to a sapphire plate and slowly cooled down to $T = 20$ K. The voltage applied to the crystal was in the range of 0.5 to 5 V; from the measured current, the dc resistivity is calculated as a function of temperature, $\rho(T)$.

To learn about the charge disproportionation in $(TMTTF)_2NO_3$, optical spectroscopy was performed utilizing a Bruker Hyperion infrared microscope attached to a Bruker Vertex 80v Fourier-transform infrared spectrometer. Reflectivity spectra $R(\omega, T)$ were collected in a frequency range from 500 to 8000 cm^{-1} between room temperature and 10 K. The optical conductivity $\sigma(\omega)$ was calculated using Kramers-Kronig analysis with constant $R(\omega)$ extrapolation below 500 cm^{-1} and ω^{-4} decay for higher frequencies. We first focused on the charge-sensitive infrared-active intramolecular vibrational mode $\nu_{28}(B_{1u})$ [26]. These measurements were performed with the light polarized along the c direction, i.e., perpendicular the main plane. As the amount of charge per TMTTF molecule is linearly related to the resonance frequency of the ν_{28} mode, charge imbalance in CO and AO states can be directly probed by tracking the peak positions upon cooling [11]. In addition, we performed reflection measurements off the crystal plane with the light polarized along the stacking direction (i.e., $E \parallel a$).

We complemented our investigations by measurements of the ESR down to low temperatures. The angular dependence of the g-factor and linewidth ΔH was obtained by a X-band

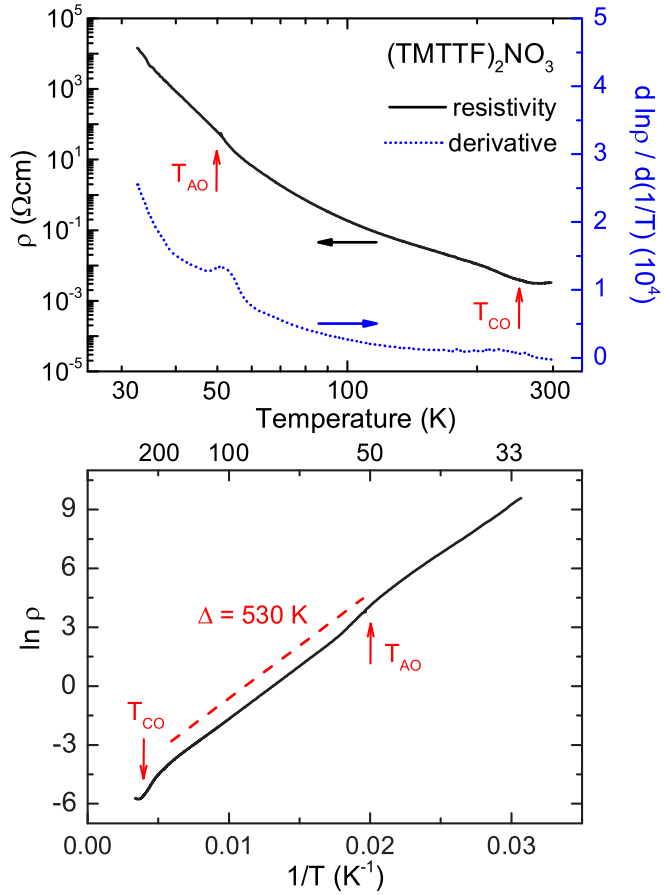

FIG. 2. Transport properties of $(TMTTF)_2NO_3$ along the chain direction a. (a) The black solid curve corresponds to the temperature dependence of the dc resistivity; note the double logarithmic scale on the left and bottom axes. The blue dotted curve gives the derivative $d \ln\rho/d(1/T)$ corresponding to the linear right axis. (b) The Arrhenius plot of the temperature-dependent resistivity allows the extraction of an activation energy $\Delta = 530$ K, indicated by the dashed red line.

spectrometer (Bruker EMXplus) as presented in detail in Ref. [21].

III. RESULTS AND ANALYSIS

A. Transport properties

The solid black curve in Fig. 2(a) represents the temperature-dependent dc resistivity of $(TMTTF)_2NO_3$ measured along the a axis; the overall behavior is reproduced on several single crystals. It is plotted in a double-logarithmic fashion to display the overall behavior. To identify the phase transitions more precisely, we calculate the derivative $d \ln \rho/d(1/T)$ and plot it as a function of temperature by the dotted blue curve [18]. A most pronounced peak in $d \ln \rho/d(1/T)$ is found at the AO transition around $T_{AO} = 50$ K. The absence of any sign of hysteresis does not conform to the standard picture of a first-order structural transition. The broad minimum of $\rho(T)$ at elevated temperature corresponds to the crossover from metal-like behavior to a charge-localized state; the zero-crossing in the derivative

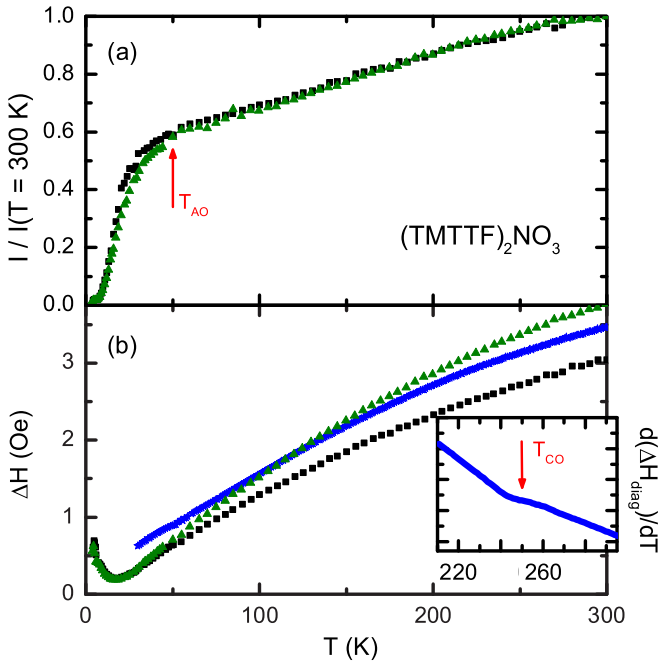

FIG. 3. ESR parameters of $(TMTTF)_2NO_3$ obtained from *X*-band measurements as a function of temperature. (a) The intensity $I(T)$ for the a and b orientation normalized to the room temperature value. The ordering of the anions at $T_{AO} = 50\,K$ causes a drop of the spin susceptibility. (b) The temperature-dependent linewidth ΔH measured along different directions: a axis (black squares), b direction (green triangles), and diagonal direction (blue stars). Strong evidence for the presence of charge order in this compound comes from the fact that at $T_{CO} = 250\,K$, the slope in the diagonal direction changes, as clearly shown in the inset, where the derivative of the smoothed data is plotted. This leads to a crossing (at around 125 K) of the temperature dependence for the linewidth obtained in the diagonal direction and the linewidth for the b orientation.

occurs at $T_\rho \approx 280\,K$, which is slightly higher than what was first reported by Coulon *et al.* [15,27]. The CO transition temperature $T_{CO} \approx 250\,K$ is best identified in the local maximum in $d \ln \rho / d(1/T)$, which occurs when the resistivity exhibits a rapid increase around 225 K. Note in $(TMTTF)_2NO_3$ salt the CO transition is more gradual compared to other Fabre salts because with decreasing anion size, the interchain separation becomes smaller, and thus one-dimensionality is less pronounced [12,28]. In Fig. 2(b), the Arrhenius plot of the resistivity is displayed, i.e., $\ln \rho(T)$ versus inverse temperature $1/T$. The CO gap Δ_{CO} can be extracted. The activated behavior continues with the same activation energy $\Delta_{CO} \approx 530\,K$ below the AO transition.

B. Magnetic properties

From our temperature-dependent *X*-band ESR experiments, we extract the intensity, resonance frequency, and the linewidth [21]. Fig. 3(a) displays the ESR intensity $I(T)$ normalized to the room temperature value I_{300K}, which corresponds to the spin susceptibility $\chi_S(T)$.

The overall behavior resembles the spin susceptibility of other $(TMTTF)_2X$ compounds [29]. The intensity monotonically decreases upon cooling from room temperature to the AO transition at $T_{AO} = 50\,K$, below which the chain dimerizes accompanied by the formation of spin singlets, leading to the observed exponential decay of $\chi_S(T)$ [14,16,20,29]. The extracted spin gap $\Delta_\sigma \approx 48\,K$ is similar for all three crystallographic directions and in agreement with previous reports [20].

At a first glance, the temperature dependence of the linewidth $\Delta H(T)$ plotted in Fig. 3(b) exhibits no distinct features along any crystallographic axes; in fact, the behavior resembles the one known from $(TMTTF)_2PF_6$ where also no kink becomes obvious at T_{CO} [13]. A closer look, however, reveals that for the diagonal orientation a change in the slope for the derivative $[d(\Delta H_{diag})/dT]$ occurs at $T_{CO} = 250\,K$, as indicated in the inset of Fig. 3. This observation is supported by the angular dependence of the ESR data reported in Ref. [21].

Here we plot the linewidth measured along the a axis, the b orientation, as well as along 45°, i.e., between the a- and the b direction. Already around $T = 250\,K$ the line of the diagonal direction is broader than expected. At $T \approx 125\,K$ the linewidth in the diagonal direction of the ab plane becomes larger than along the a and b directions. This is taken as an indication that a CO transition is present in $(TMTTF)_2NO_3$.

C. Vibrational spectroscopy

Out of the molecular vibrations in TMTTF, three modes are most sensitive to the charge per molecule. Two of them are totally symmetric A_g (ν_3 and ν_4), and as a result they are infrared inactive; however, they become visible via electron-molecular vibrational (emv) coupling [11]. The third one is an asymmetric infrared active B_{1u} (ν_{28}) mode which can be probed in out-of-plane direction (i.e., $E \parallel c$ axis). It exhibits a linear shift of the resonance frequency with ionicity of the TMTTF molecule due to the strengthening/loosening of the intramolecular bonds. The rather large intensity and weak coupling to the electronic background makes it ideal for investigation of the charge distribution. In the normal state, each TMTTF molecule contains the net charge $\rho = +0.5e$, which corresponds to one peak in the infrared spectra ($\nu^{+0.5} = 1547\,cm^{-1}$).

In Fig. 4(a) the development of the $\nu_{28}(B_{1u})$ mode is shown as the $(TMTTF)_2NO_3$ crystal is cooled down. While at room temperature we observe only one broad band that cannot be sensibly separated, two peaks are clearly distinguished below $T = 250\,K$. The ν_{28} mode in $(TMTTF)_2NO_3$ is much broader compared to corresponding features observed in compounds with octahedral anions [11] and comparable to those seen for compounds with tetrahedral anions [19]. This can be attributed to the inherent disorder of the anions. To analyze the data quantitatively, we fit the ν_{28} mode using two Lorentz oscillators, which works reasonably well up to T_{CO}. In Fig. 4(b) the resonance frequencies are depicted as a function of temperature. Due to the increasing linewidth and diminishing intensity, it was not possible to reliably separate two contributions above 250 K, as illustrated in Fig. 5.

The absence of a sensible fit is indicated by the shaded area. Note, that this is a gradual process resembling a continuous second-order phase transition. In addition, we can identify a simultaneous upshift of both modes by less than 1 cm^{-1} as

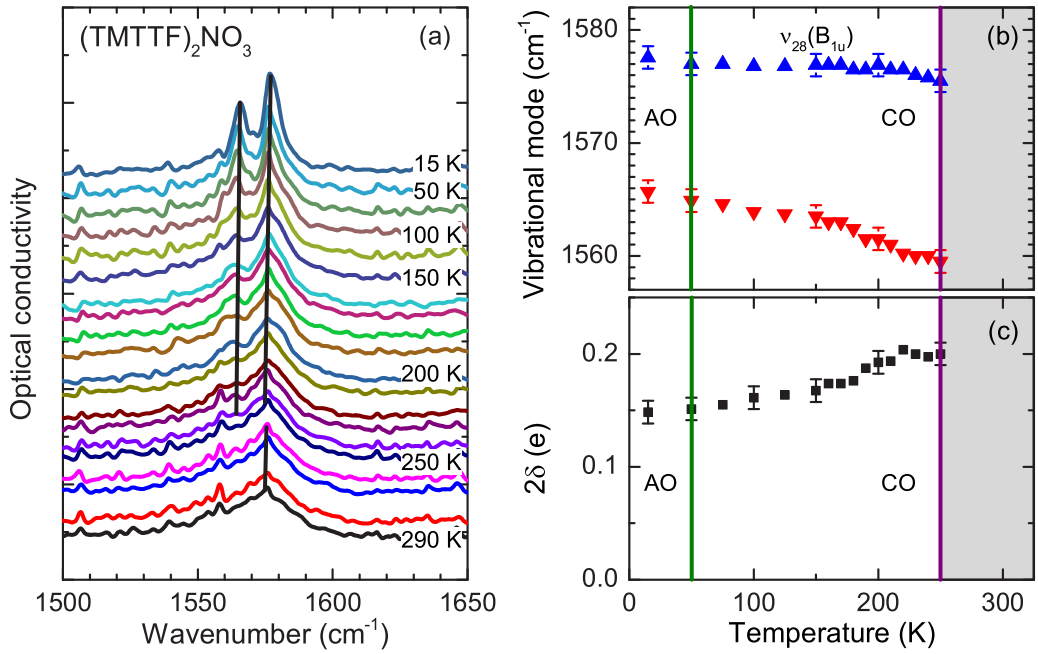

FIG. 4. (a) Temperature evolution of the charge-sensitive infrared-active molecular vibration ν_{28} observed in the mid-infrared spectra of $(TMTTF)_2NO_3$ for $E \parallel c$. For clarity reasons, the curves are shifted with respect to each other. (b) Resonance frequency of the $\nu_{28}(B_{1u})$ mode as a function of temperature obtained from fitting the spectra with two Lorentzians below T_{CO} (blue and red triangles). The error bars represent the uncertainty of the fit procedure; more important, however, the peaks gradually diminish on raising the temperature and cannot be reliably distinguished above $T_{CO} = 250$ K as demonstrated in Fig. 5. The gray area indicates that we present the fit results only below 250 K. The overall behavior resembles a gradual phase transition more than a rapid jump common to first-order transition. Note the slight upward shift for $T < T_{AO}$. (c) By using Eq. (1) the charge imbalance 2δ can be directly calculated from the peak separation $\Delta\nu$.

the AO state is entered below 50 K; also, the intensity of the modes increases. From the positions of the two peaks, the charge imbalance 2δ can be calculated via

$$2\delta = \frac{\Delta\nu}{80\,\mathrm{cm}^{-1}}, \tag{1}$$

where $\Delta\nu$ is the spectral separation between the peaks in the CO state.

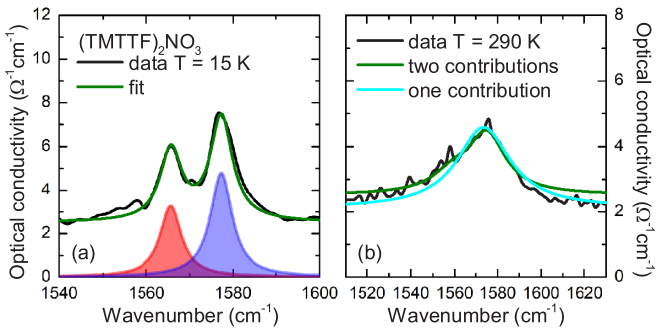

FIG. 5. Vibrational spectra of $(TMTTF)_2NO_3$ in the range of the ν_{28} mode. (a) The 15 K spectrum can be readily fitted with two Lorentzians, indicated by the red and blue curves; the overall fit is represented by the green line. (b) At $T = 290$ K the curve is much broader (note, the frequency scale differs by a factor of 2) and the mode is less pronounced. We present a fit of the data with one contribution (cyan line) and two contributions (green line) and conclude that a two-component fit is not sensible.

The temperature dependence of $2\delta(T)$ is plotted as a function of temperature in Fig. 4(c). It becomes obvious at $T_{CO} = 250$ K and reaches the maximum $2\delta = (0.21 \pm 0.01)e$ at 220 K; this perfectly matches the temperatures obtained from the transport data [Fig. 2(a)]. The charge disproportionation then gradually decreases to $0.15e$ and remains unchanged in the AO state.

IV. DISCUSSION

A. Charge order transtition

In the case of Fabre salts with highly symmetric anions, such as $(TMTTF)_2SbF_6$ and $(TMTTF)_2AsF_6$, a noticeable kink in the ESR linewidth has been identified at T_{CO} [13]. The charge disproportionation on the TMTTF molecules leads to nonequivalent couplings between the anions and the TMTTF molecules that influences the magnetic behavior of the spin chain. The ESR linewidth of $(TMTTF)_2NO_3$, however, barely changes at T_{CO}; only a plateau in the derivative is identified in the inset of Fig. 3.

The low-temperature optical spectra of $(TMTTF)_2NO_3$ displayed in Fig. 4(a) contain two vibrational features corresponding to ν_{28} that reflect the presence of two TMTTF sites containing nonequivalent charges; the strength of the low-frequency feature gradually diminishes upon warming up, can barely be resolved above 200 K, and becomes undistinguishable around T_{CO}. Traces of charge disproportionation might be already present at room temperature, as observed in some BEDT-TTF compounds [30,31], for instance; however, the width of the vibrational band and the weakness of

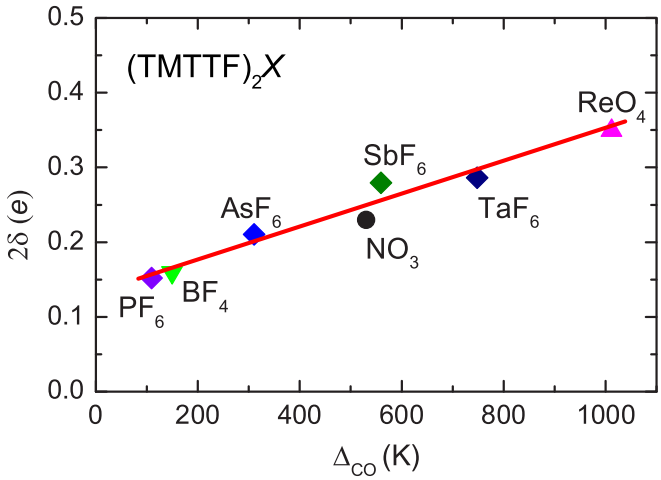

FIG. 6. Amount of charge disproportionation 2δ plotted versus the charge-order gap Δ_{CO} obtained from temperature-dependent transport measurements [9,12]. The red line indicates the linear dependence between 2δ and Δ_{CO}.

the second feature does not allow a firm conclusion. Beyond this uncertainty, $2\delta(T)$ continuously decreases when cooling below T_{CO} before it saturates around $0.15e$, as depicted in Fig. 4(c). It stays almost the same in the AO state, and we can conclude that the effect of the AO on charge distribution is rather small.

From a comparative study [19], Pustogow *et al.* concluded that the CO state in $(TMTTF)_2X$ salts with octahedral and tetrahedral anions is determined by the stacking of the organic molecules and independent on symmetry of the anions. In other words, the CO state is only governed by the competition between intersite Coulomb repulsion V on the one hand and overlap integral t or bandwidth W on the other hand. In first approximation, the charge imbalance 2δ should be proportional to the charge gap Δ_{CO} and to the effective correlations V/W. In the corresponding plot, Fig. 6, we illustrate that $(TMTTF)_2NO_3$ nicely follows the linear dependence between 2δ obtained from vibrational spectroscopy and Δ_{CO} extracted from the transport measurements. This observation suggests that the CO state is mainly driven by Coulomb repulsion that occurs from charge imbalance between neighboring sites in the organic stack. Here the anion potential seems to play only a minor role. Interestingly, $(TMTTF)_2NO_3$ does not follow the general relation between T_{CO} and 2δ [19]; as a matter is fact, the CO transition occurs at about twice the temperature as expected.

B. Anion order

At elevated temperatures the anions of Fabre salts are randomly oriented; due to entropy reasons, the noncentrosymmetric anions prefer to become oriented on cooling. The increasing charge disproportionation on the TMTTF stacks below T_{CO} and their coupling to the anions, however, is not sufficient to completely order the anions. From our dc resistivity measurements (Fig. 2), we see that the AO transition takes place only at $T_{AO} = 47$ K, in coarse agreement with previous results [15,16]. Although this is a structural transition, we do not observe a hysteresis in the resistivity data, in accord with previous results [32,33]. The small size of the NO_3^- anion might be one reason why the phase transition inclines toward second order. This also implies a weak coupling to the TMTTF molecules and minor influence on the electronic properties of $(TMTTF)_2NO_3$, as seen in the insignificant change of the resistivity below $T_{AO} = 47$ K.

The particular shape and the small size of the NO_3^- anions explain why the T_{AO} is far below the transition temperature observed in $(TMTTF)_2ReO_4$ (157K) and $(TMTTF)_2ClO_4$ (73.4K) which contain much larger anions. The other Fabre salt with tetrahedral anion, $(TMTTF)_2BF_4$, seems to make an exception, with $T_{AO} = 41.5$ K. For tetrahedral anions, sulfur-ligand interactions govern the charge distribution in the AO state, while for $(TMTTF)_2NO_3$ -$CH_3\cdots O$, interactions are more important; we will come back to this in Section IV C. In the case of the planar NO_3^- anions, the three-dimensional rotation of the entire molecule might be frozen at much higher temperatures, for instance at T_{CO} – while rotation within the pane continues down to T_{AO}.

It is interesting to note that both branches of the $\nu_{28}(A_g)$ vibrational mode reveals a slight upshift at T_{AO}, as seen in Fig. 4(b). This could indicate a minute reduction in the overall charge transfer, or it indicates a general stiffening of the vibrational pattern due to interaction with the anion, which move closer to the TMTTF molecules.

A deeper insight into the AO is gained by looking at the vibrations of the NO_3^- anions. The out-of-plane bending mode ν_2 shows up rather prominently around $810-820$ cm^{-1} [34,35]. From the temperature dependence of this fundamental mode plotted in Fig. 7, we observe a clear splitting below $T_{AO} = 50$ K. This could simply be explained by a distortion of the NO_3^- anions at the transition resulting in breaking of the triangular symmetry. But we can also imagine different amounts of charge on the anions in their ordered state; in other words, the AO causes some CO in the NO_3^- chain. This is a result of the alternating coupling to the TMTTF molecules, leading to a tetramerization there.

C. Tetramerization

The $(TMTTF)_2X$ stoichiometry already imposes a dimerization onto the TMTTF stacks, as depicted in Fig. 1(a). The AO with a wave vector $(\frac{1}{2}, 0, 0)$ leads to a tetramerization in the $(TMTTF)_2NO_3$ salt, i.e., a doubling of the unit cell along the a axis [Fig. 1(b)]. Importantly, this is not just a structural order due the alternating orientation of the anions but also a shift of the anions within the methyl-group cavity. Furthermore it affects the link toward the S atom and rearranges the charges [19,36]. Due to the small size and minor shift of the NO_3^- anions, this structural alternation is quite weak compared to other $(TMTTF)_2X$ salts, nevertheless it is a crucial phenomenon even in the present case. For the sister compound $(TMTSF)_2NO_3$ – where sulfur atoms are substituted by Se – the AO transition is very similar and the wave vector is identical. It was shown for this compound [37] that the -$CH_3\cdots O$ interactions are important; the anion reorientation below T_{AO} and the shift toward selected methyl groups cause a change of the charge pattern, where donors with shorter -$CH_3\cdots O$ distances are more positively charged

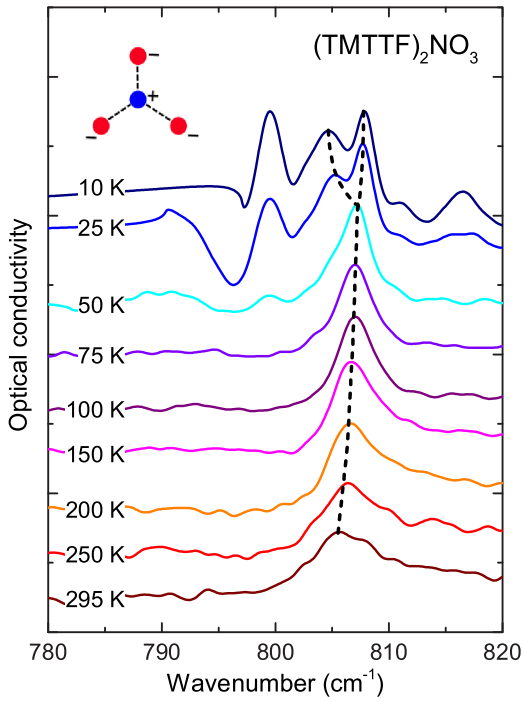

FIG. 7. Temperature evolution of the optical conductivity in the region of the fundamental ν_2 mode of NO_3^- anion measured for $E \parallel c$ axis. The curves are displaced for clarity. The dashed black line tracks the resonance frequency of the ν_2 molecular vibration upon cooling and visualizes the splitting below $T_{AO} = 50$ K.

(charge rich), while donors with smaller -$CH_3 \cdots$O distances are charge poor [24,25,38]. We do expect a similar behavior for $(TMTTF)_2NO_3$; the uniform charge distribution at elevated temperatures becomes alternated below T_{CO} presumably by the nearest-neighbor Coulomb repulsion V. In a second step, this 1010 alternation will change to a 0110 pattern in the AO state, as depicted in Fig. 8.

This corresponds exactly to the charge disproportionation within the NO_3^- anions, inferred from Fig. 7; below T_{AO}, the

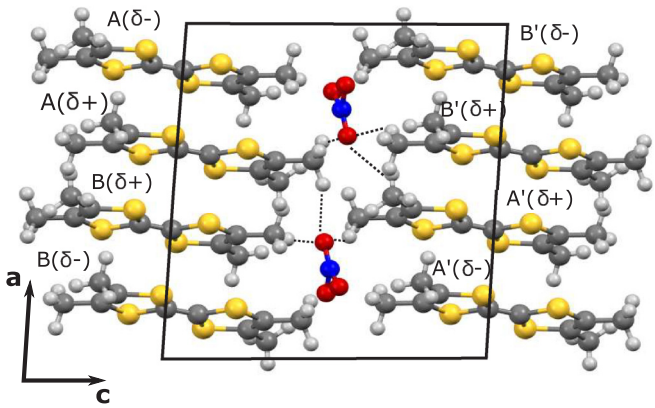

FIG. 8. Sketch of the $(TMTTF)_2NO_3$ tetramer in the CO and AO state at low temperatures. Here the dimers A and A′, as well as B and B′, are linked via inversion symmetry. The dashed lines indicate the shortest -$CH_3 \cdots$O distances; $(\delta+)$ corresponds to the charge-rich sites and $(\delta-)$ to the charge-poor ones, forming a 0110 pattern along the a direction.

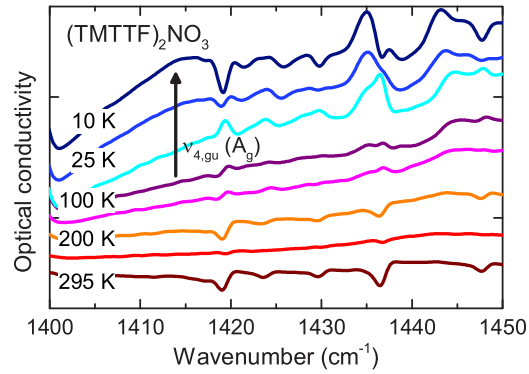

FIG. 9. Temperature dependence of the mid-infrared spectra of $(TMTTF)_2NO_3$ probed with $E \parallel a$. Around 1410 to 1420 cm^{-1} the $\nu_{4,gu}(A_g)$ mode becomes activated by the tetramerization in the AO state.

fundamental vibrational modes split because every second anion becomes charge rich while the others are depleted.

An unambiguous proof of the tetramerization along the stacks is given in Fig. 9, where the appearance of the $\nu_4(A_g)$ vibration of the TMTTF molecule is observed as $T < T_{AO}$. This fully symmetric mode is typically seen in Raman spectroscopy but infrared silent [11]; however, an out-of-phase coupling can make them infrared active. In the present case, AO activates the dimeric in-phase vibration by out-of-phase combination of two dimers within the tetramer; the $\nu_{4,gu}$ mode couples to infrared light via the a dipole between the dimers [19]. In Fig. 9 we see this feature at around 1410 cm^{-1} appearing in the $E \parallel a$ spectra below 50 K. Compared to other Fabre salts with noncentrosymmetric anions, the intensity of this mode is relatively small, but this is consistent with the fact that tetramerization in $(TMTTF)_2NO_3$ is rather weak. With growing anion size $d(NO_3) < d(BF_4) < d(ClO_4) < d(ReO_4)$, the tetramerization is more pronounced and the intensity of the $\nu_{4,gu}$ mode increases. This supports the assumption that the 0110 charge arrangement in the AO state is mainly due to the anionic potential and anion arrangement, while the CO state is governed by nearest-neighbor Coulomb repulsion.

In Fig. 2 we have demonstrated that the AO transition affects the transport properties as a slight kink at T_{AO}, but does not lead to drastic step with a hysteretic behavior. The activation energy remains unchanged and only some offset is observed; in other words, the physical state above T_{AO} is very similar to the low-temperature phase. The tetramerization on the TMTTF stack is most prominent in ESR properties [14–16,21] where spin singlets are formed below T_{AO} leading to an exponential decay of the spin susceptibility, as presented in Fig. 3. From the corresponding fit we obtain a spin gap $\Delta_\sigma \approx 48$ K in full accord with previous observations. It is interesting to note that the phase transition occurs much more gradually compared with $(TMTTF)_2BF_4$ or $(TMTTF)_2ReO_4$ [13], for instance.

V. CONCLUSIONS

Detailed transport, ESR, and infrared studies on $(TMTTF)_2NO_3$ were performed to explore the charge-ordered

and AO states in this salt. From the different methods we independently determine the CO transition at $T_{CO} \approx 250\,K$ with a charge imbalance of $2\delta = 0.2e$. Our findings suggest that the charge disproportionation in the CO state is mainly governed by intersite Coulomb repulsion and solely determined by the TMTTF stacks. The universal dependence between the charge imbalance 2δ and the size of the CO gap Δ_{CO} also holds for $(TMTTF)_2NO_3$. In the AO state the NO_3^- anions order in an alternating fashion. Due to the $\text{-}CH_3 \cdots O$ interaction charge pattern changes toward 0110 below $T_{AO} = 50\,K$. This causes not only a step in the dc resistivity but also most prominent the formation of spin singlets, leading to an exponential drop in the spin susceptibility.

ACKNOWLEDGMENTS

We acknowledge the support by the Deutsche Forschungsgemeinschaft and appreciate helpful discussions with A. Pustogow.

[1] T. Giamarchi, *Quantum Physics in One Dimension* (Oxford University Press, Oxford, 2004).

[2] D. Baeriswyl and L. Degiorgi (editors), *Strong Interactions in Low Dimensions*, Physics and chemistry of materials with low-dimensional structures (Kluwer Academic, Dordrecht, 2004), Vol. 25.

[3] D. Jérome and H.-J. Schulz, Organic conductors and superconductors, Adv. Phys. **31**, 299 (1982).

[4] J.-P. Farges (editor), *Organic Conductors* (Marcel Dekker, New York, 1994).

[5] M. Dressel, Spin-charge separation in quasi one-dimensional organic conductors, Naturwissenschaften **90**, 337 (2003); Ordering phenomena in quasi-one-dimensional organic conductors, **94**, 527 (2007).

[6] J.-P. Pouget, P. Alemany, and E. Canadell, Donor-anion interactions in quarter-filled low-dimensional organic conductors, Mater. Horiz. **5**, 590 (2018).

[7] S. Tomić and M. Dressel, Ferroelectricity in molecular solids: a review of electrodynamical properties, Rep. Prog. Phys. **78**, 096501 (2015); M. Dressel and S. Tomić, Molecular quantum materials, Adv. Phys. **69**, 1 (2020).

[8] R. Laversanne, C. Coulon, B. Gallois, J. Pouget, and R. Moret, Structural and electrical properties of $(TMTTF)_2MF_6$ salts (M = P, As, Sb). Rôle of the anions, J. Phys. Lett. (France) **45**, L393 (1984).

[9] D. S. Chow, F. Zamborszky, B. Alavi, D. J. Tantillo, A. Baur, C. A. Merlic, and S. E. Brown, Charge ordering in the TMTTF family of molecular conductors, Phys. Rev. Lett. **85**, 1698 (2000); F. Zamborszky, W. Yu, W. Raas, S. E. Brown, B. Alavi, C. A. Merlic, and A. Baur, Competition and coexistence of bond and charge orders in $(TMTTF)_2AsF_6$, Phys. Rev. B **66**, 081103(R) (2002); W. Yu, F. Zhang, F. Zamborszky, B. Alavi, A. Baur, C. A. Merlic, and S. E. Brown, Electron-lattice coupling and broken symmetries of the molecular salt $(TMTTF)_2SbF_6$, *ibid.* **70**, 121101(R) (2004).

[10] P. Monceau, F. Y. Nad, and S. Brazovskii, Ferroelectric Mott-Hubbard Phase of Organic $(TMTTF)_2X$ Conductors, Phys. Rev. Lett. **86**, 4080 (2001); F. Nad and P. Monceau, Dielectric response of the charge ordered state in quasi-one-dimensional organic conductors, J. Phys. Soc. Jpn. **75**, 051005 (2006); P. Monceau, Electronic crystals: an experimental overview, Adv. Phys. **61**, 325 (2012).

[11] M. Dumm, B. Salameh, M. Abaker, L. K. Montgomery, and M. Dressel, Magnetic and optical studies of spin and charge ordering in $(TMTTF)_2AsF_6$, J. Phys. IV (France) **114**, 57 (2004); M. Dumm, M. Abaker, and M. Dressel, Mid-infrared response of charge-ordered quasi-1D organic conductors $(TMTTF)_2X$, *ibid.* **131**, 55 (2005); M. Dressel, M. Dumm, T. Knoblauch, and M. Masino, Comprehensive optical investigations of charge order in organic chain compounds $(TMTTF)_2X$, Crystals **2**, 528 (2012).

[12] Y. Oka, N. Matsunaga, K. Nomura, A. Kawamoto, K. Yamamoto, and K. Yakushi, Charge order in $(TMTTF)_2TaF_6$ by infrared spectroscopy, J. Phys. Soc. Jpn. **84**, 114709 (2015).

[13] T. Nakamura, Possible charge ordering patterns of the paramagnetic insulating states in $(TMTTF)_2X$, J. Phys. Soc. Jpn. **72**, 213 (2003); K. Furukawa, T. Hara, and T. Nakamura, Deuteration effect and possible origin of the charge-ordering transition of $(TMTTF)_2X$, *ibid.* **74**, 3288 (2005); Y. Nogami, T. Ito, K. Yamamoto, N. Irie, S. Horita, T. Kambe, N. Nagao, K. Oshima, N. Ikeda, and T. Nakamura, X-ray structural study of charge and anion orderings of TMTTF salts, J. Phys. IV France **131**, 39 (2005); F. Iwase, K. Sugiura, K. Furukawa, and T. Nakamura, ^{13}C NMR study of the magnetic properties of the quasi-one-dimensional conductor $(TMTTF)_2SbF_6$, Phys. Rev. B **84**, 115140 (2011); B. Salameh, S. Yasin, M. Dumm, G. Untereiner, L. Montgomery, and M. Dressel, Spin dynamics of the organic linear chain compounds $(TMTTF)_2X$ (X = SbF_6, AsF_6, BF_4, ReO_4, and SCN), *ibid.* **83**, 205126 (2011); S. Yasin, B. Salameh, E. Rose, M. Dumm, H.-A. Krug von Nidda, A. Loidl, M. Ozerov, G. Untereiner, L. Montgomery, and M. Dressel, Broken magnetic symmetry due to charge-order ferroelectricity discovered in $(TMTTF)_2X$ salts by multifrequency esr, *ibid.* **85**, 144428 (2012); M. Dressel, M. Dumm, T. Knoblauch, B. Köhler, B. Salameh, and S. Yasin, Charge order breaks magnetic symmetry in molecular quantum spin chains, Adv. Condens. Matter Phys. **2012**, 398721 (2012).

[14] C. Coulon, A. Maaroufi, J. Amiell, E. Dupart, S. Flandrois, P. Delhaes, R. Moret, J. P. Pouget, and J. P. Morand, Antiferromagnetic and structural instabilities in tetramethyltetrathiafulvalene thiocyanate $[(TMTTF)_2SCN]$, Phys. Rev. B **26**, 6322 (1982).

[15] C. Coulon, P. Delhaes, S. Flandrois, R. Lagnier, E. Bonjour, and J. Fabre, A new survey of the physical properties of the $(TMTTF)_2X$ series. role of the counterion ordering, J. Phys. (France) **43**, 1059 (1982).

[16] R. Moret, J. Pouget, R. Comes, and K. Bechgaard, Structural phase transitions in the $(TMTSF)_2X$ and $(TMTTF)_2X$ series: A survey with some new results, J. Phys. (France) Coll. **44**, C3-957 (1983).

[17] J. Pouget, R. Moret, R. Comes, K. Bechgaard, J. Fabre, and L. Giral, X-ray diffuse scattering study of some $(TMTSF)_2X$ and $(TMTTF)_2X$ salts, Mol. Cryst. Liq. Cryst. **79**, 485 (1982); S. Ravy, R. Moret, J. Pouget, and R. Comes, Structural phase transitions in $(TMTSF)_2X$ and related compounds, Synth. Met. **13**, 63 (1986).

[18] R. Rösslhuber, E. Rose, T. Ivek, A. Pustogow, T. Breier, M. Geiger, K. Schrem, G. Untereiner, and M. Dressel, Structural and electronic properties of $(TMTTF)_2X$ salts with tetrahedral anions, Crystals **8**, 121 (2018).

[19] A. Pustogow, T. Peterseim, S. Kolatschek, L. Engel, and M. Dressel, Electronic correlations versus lattice interactions: Interplay of charge and anion orders in $(TMTTF)_2X$, Phys. Rev. B **94**, 195125 (2016).

[20] C. Coulon, P. Foury-Leylekian, J.-M. Fabre, and J.-P. Pouget, Electronic instabilities and irradiation effects in the $(TMTTF)_2X$ series, Eur. Phys. J. B **88**, 85 (2015).

[21] L. N. Majer, B. Miksch, G. G. Lesseux, G. Untereiner, and M. Dressel, Charge-order phase transition in the quasi one-dimensional organic conductor $(TMTTF)_2NO_3$, Appl. Magn. Res. **51**, 1321 (2020).

[22] B. Köhler, E. Rose, M. Dumm, G. Untereiner, and M. Dressel, Comprehensive transport study of anisotropy and ordering phenomena in quasi-one-dimensional $(TMTTF)_2X$ salts ($X = PF_6$, AsF_6, SbF_6, BF_4, ClO_4, ReO_4), Phys. Rev. B **84**, 035124 (2011).

[23] B. Liautard, S. Peytavin, G. Brun, and M. Maurin, Etude structurale du nitrate de tétraméthyltétrathiafulvaléne $(TMTTF)_2NO_3$, Acta Crystall. B **38**, 2746 (1982).

[24] Y. Barrans, J. Gaultier, S. Bracchetti, P. Guionneau, D. Chasseau, and J. Fabre, Low temperature structural properties of the $(TMTSF)_2NO_3$ salt, Synth. Met. **103**, 2042 (1999).

[25] B. Guster, M. Pruneda, P. Ordejón, E. Canadell, and J.-P. Pouget, Anion ordering transition and fermi surface electron–hole instabilities in the $(TMTSF)_2ClO_4$ and $(TMTSF)_2NO_3$ bechgaard salts analyzed through the first-principles Lindhard response function, J. Phys.: Condens. Matter **33**, 085705 (2020).

[26] M. Meneghetti, R. Bozio, I. Zanon, C. Pecile, C. Ricotta, and M. Zanetti, Vibrational behavior of molecular constituents of organic superconductors: TMTSF, its radical cation and the sulfur analogs TMTTF and $TMTTF^+$, J. Chem. Phys. **80**, 6210 (1984).

[27] We could reproduce our findings on several single crystals and obtain quantitative agreement better than 1–2%. The discrepancy to the data of 1982 by Coulon *et al.* [15] is within the typical variation found among crystals of different laboratories using different growth conditions, solvents, purification, etc. Note that here we consider a shallow resistivity minimum due to a crossover from barely metallic to more localized charge transport, while there is a very good agreement as far as the anion ordering transition is concerned.

[28] T. Knoblauch and M. Dressel, Charge disproportionation in $(TMTTF)_2X$ ($X = PF_6$, AsF_6 and SbF_6) investigated by infrared spectroscopy, Phys. Status Solidi C **9**, 1158 (2012).

[29] M. Dumm, A. Loidl, B. W. Fravel, K. P. Starkey, L. K. Montgomery, and M. Dressel, Electron spin resonance studies on the organic linear-chain compounds $TMTCF_2X$ ($C = S$, Se; $X = PF_6$, AsF_6, ClO_4, Br)), Phys. Rev. B **61**, 511 (2000); M. Dumm, A. Loidl, B. Alavi, K. P. Starkey, L. K. Montgomery, and M. Dressel, Comprehensive esr study of the antiferromagnetic ground states in the one-dimensional spin systems $(TMTSF)_2PF_6$, $(TMTSF)_2AsF_6$, and $(TMTTF)_2Br$, *ibid.* **62**, 6512 (2000).

[30] T. Ivek, B. Korin-Hamzić, O. Milat, S. Tomić, C. Clauss, N. Drichko, D. Schweitzer, and M. Dressel, Electrodynamic response of the charge ordering phase: Dielectric and optical studies of α-$(BEDT\text{-}TTF)_2I_3$, Phys. Rev. B **83**, 165128 (2011).

[31] A. Pustogow, Y. Saito, A. Rohwer, J. A. Schlueter, and M. Dressel, Coexistence of charge order and superconductivity in β''-$(BEDT\text{-}TTF)_2SF_5CH_2CF_2SO_3$, Phys. Rev. B **99**, 140509(R) (2019); A. Pustogow, K. Treptow, A. Rohwer, Y. Saito, M. Sanz Alonso, A. Löhle, J. A. Schlueter, and M. Dressel, Charge order in β''-phase BEDT-TTF salts, *ibid.* **99**, 155144 (2019).

[32] J.-P. Pouget and S. Ravy, Structural aspects of the Bechgaard salts and related compounds, J. Phys. I (France) **6**, 1501 (1996).

[33] J.-P. Pouget, Structural aspects of the Bechgaard and Fabre salts: An update, Crystals **2**, 466 (2012).

[34] J. L. Stewart, The infrared spectrum of the nitrate ion in various crystalline environments, Master's thesis, Oregon State University, Corvallis, Oregon, 1965.

[35] J.-P. Mathieu and M. Lounsbury, The Raman spectra of metallic nitrates and the structure of concentrated solutions of electrolytes, Disc. Faraday Soc. **9**, 196 (1950).

[36] D. Le Pévelen, J. Gaultier, Y. Barrans, D. Chasseau, F. Castet, and L. Ducasse, Temperature and pressure dependencies of the crystal structure of the organic superconductor $(TMTSF)_2ClO_4$, Eur. Phys. J. B **19**, 363 (2001).

[37] T. J. Emge, M. A. Beno, C. A. Daws, H. H. Wang, and J. M. Williams, Novel structural features, and their relationship to the electrical properties, of the organic conductor $(TMTSF)_2NO_3$ at 298 K and 125 K, Mol. Cryst. Liq. Cryst. **116**, 153 (1984).

[38] P. Alemany, J.-P. Pouget, and E. Canadell, Electronic structure and anion ordering in $(TMTSF)_2ClO_4$ and $(TMTSF)_2NO_3$: A first-principles study, Phys. Rev. B **89**, 155124 (2014).